Journal of Alloys and Compounds 509 (2011) 6930–6934

Contents lists available at ScienceDirect

Journal of Alloys and Compounds

journal homepage: www.elsevier.com/locate/jallcom

Preparation and characteristics of Fe_3O_4@YVO_4:Eu^{3+} bifunctional magnetic–luminescent nanocomposites

Hongxia Peng, Guixia Liu*, Xiangting Dong, Jinxian Wang, Jia Xu, Wensheng Yu

School of Chemistry and Environmental Engineering, Changchun University of Science and Technology, Changchun 130022, China

ARTICLE INFO

Article history:
Received 24 December 2010
Received in revised form 30 March 2011
Accepted 1 April 2011
Available online 7 April 2011

Keywords:
Fe_3O_4
YVO_4:Eu^{3+}
Core–shell
Magnetic–luminescent materials

ABSTRACT

A facile direct precipitation method has been developed for the synthesis of bifunctional magnetic–luminescent nanocomposites with Fe_3O_4 nanoparticles as the core and YVO_4:Eu^{3+} as the shell. Transmission electron microscopy (TEM) images revealed that the obtained bifunctional nanocomposites had a core–shell structure and a spherical morphology. The average size was ~150 nm, and the thickness of the shell was ~15 nm. The X-ray diffraction (XRD) patterns showed that a cubic spinel structure of Fe_3O_4 core and a tetragonal phase of YVO_4 shell were obtained. Fourier transform infrared (FT-IR) spectra confirmed that the YVO_4:Eu^{3+} had been successfully deposited on the surface of Fe_3O_4 nanoparticles. Photoluminescence (PL) spectra indicated that the nanocomposites displayed a strong red characteristic emission of Eu^{3+}. Magnetic measurements showed that the obtained bifunctional nanocomposites exhibited superparamagnetic behavior at room temperature. Therefore, the bifunctional nanocomposites are expected to develop many potential applications in biomedical fields.

1. Introduction

Magnetic nanoparticles have been extensively studied in the fields of biomedical applications, including magnetic resonance imaging (MRI), gene/drug delivery, and biosensors, as well as biochemical separation and concentration of trace amount of samples [1–14]. Luminescent nanoparticles have attracted great attention in the field of biological labeling [15–18]. Although superparamagnetic and luminescent nanoparticles have their own distinguish properties, and cannot be replaced with each other, and they cannot show the multiple functions if they are used by themselves [19–22]. It is necessary to constitute a multifunctional nanoplatform by integrating multiple nanoparticle components into a single nanosystem by rational assembly and hybridization techniques. Magnetic–luminescent bifunctional materials have attracted great attention in recent years due to their increasingly important applications in biomedical research, clinical diagnosis, and biomedicine [23–28]. For example, Corato et al. first synthesised the mixture of magnetic nanoparticles, quantum dots, and an amphiphilic polymer, followed by modifying the surface with folic acid molecules to prepare trifunctional polymer nanobeads [23]. Liu et al. employed a novel process of combining emulsification with layer-by-layer self-assembly techniques to synthesize highly magnetic–luminescent alginate–templated composite microparticles [24]. Kas et al. employed the ligand-exchange mechanism in a simple and versatile extraction method to synthesize hybrid nanoparticles composed of luminescent quantum dots and superparamagnetic iron oxides [25]. Sun et al. synthesized Fe_3O_4/CdTe magnetic/fluorescent nanocomposites that applied to the immunolabeling and fluorescent imaging of cancer cells [26]. Wang et al. prepared biodegradable magnetic–fluorescent magnetite/poly (DL-lactic acid-co-a,b-malic acid) composite nanoparticles that applied to stem cell labeling [27]. Wang et al. synthesized magnetic and luminescent Fe_3O_4/CdTe nanocomposites with an average diameter of 40–50 nm, yellow-green emission feature and room temperature ferro-magnetism [28]. The magnetic–luminescent nanocomposites allow not only external manipulation with a magnetic field but also real time visualization with fluorescence imaging techniques [29–33]. The use of bifunctional magnetic and luminescent nanoplatforms will further improve diagnostic effectiveness and reduce side effects [34–37].

Most of the magnetic–luminescent nanocomposites are core–shell structures with the great majority of emitters being either organic dyes or quantum dots (QDs). However, organic dyes typically exhibit rapid photobleaching and a low fluorescence quantum yield, while QDs are less chemically stable and potentially toxic, show fluorescence intermittence [38–43]. Therefore, such intrinsic disadvantages would seriously hinder their application in the biomedical field, especially for use in human body [44–46]. In addition to organic dyes and QDs, lanthanide-doped nanoparticles are gaining popularity and have been recognized as a promising

* Corresponding author. Tel.: +86 431 85582574; fax: +86 431 86176292.
E-mail address: liuguixia22@yahoo.com.cn (G. Liu).

0925-8388/$ – see front matter © 2011 Elsevier B.V. All rights reserved.
doi:10.1016/j.jallcom.2011.04.004

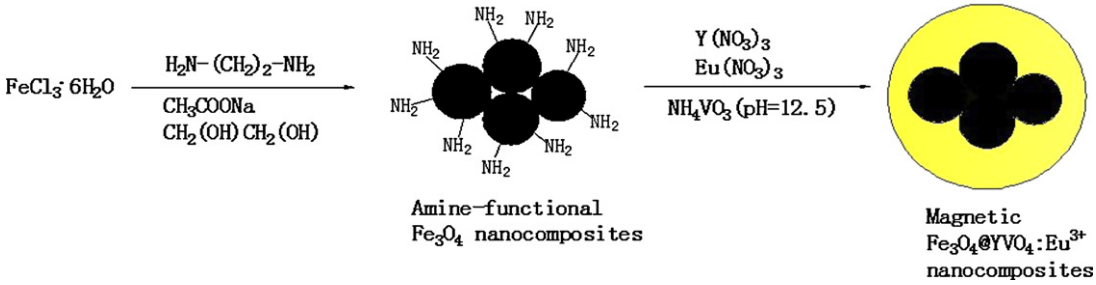

Scheme 1. Synthetic strategy for the Fe_3O_4@YVO_4:Eu^{3+} nanocomposites.

new class of fluorescent biological label due to their unique luminescence properties, such as large Stokes shifts, narrow linewidth emission bands, long lifetimes and superior photostability [47,48]. Contrasted with semi-conductor QDs, the emission wavelength of the lanthanide nanoparticles is independent of particle size [49]. Furthermore, surface modification does not significantly affect their optical properties, because their luminescence arises as a result of electronic transitions of the lanthanide ions. In particular, they also possess excellent chemical stability, high quantum yield and probably low toxicity [50,51]. YVO_4 is an important host crystal for lanthanide-doped phosphors. It provides a wide band gap (>10 eV) and suitable Y^{3+} sites where trivalent rare-earth ions can be easily substituted without additional charge compensation [52,53]. Furthermore, YVO_4 is an efficient UV phosphor in the near-UV region [54].

To the best of our knowledge, there are few reports on the synthesis of bifunctional magnetic–luminescent nanocomposites with Fe_3O_4 nanoparticles as the core and lanthanide-doped nanoparticles as the shell. Sun et al. employed the hydrothermal method to synthesize $Fe_3O_4/SiO_2/YVO_4$:Eu^{3+}magnetic/luminescent nanocomposites [47]. Wang et al. employed the layer-by-layer (LbL) technique to fabricate the Fe_3O_4@LaF_3:Ce^{3+},Tb^{3+} bifunctional nanocomposites [48]. Yang et al. employed the sol–gel method to prepare Fe_3O_4@$nSiO_2$@$mSiO_2$@YVO_4:Eu^{3+} bifunctional nanocomposites [49]. Zhang et al. employed the homogeneous precipitation to synthesize Fe_3O_4@SiO_2/Y_2O_3:Tb bifunctional nanocomposites [50]. In these methods, there are three steps for preparing the core–shell nanocomposites. The first step is the preparation of magnetic core, then the surface functional treatment of the core and finally coating the shell on the core. The synthesis process is inconvenient and the cost is high, and the feature of the core should be changed in the surface treatment process. Therefore, it is a disadvantage for the obtaining of ideal product.

In this work, we report the development of a facile two-step method for the preparation of bifunctional magnetic–luminescent nanocomposites. Firstly, amino-functional magnetic Fe_3O_4 nanoparticles were solvothermally prepared as the cores. Secondly, YVO_4:Eu^{3+} luminescent particles were coated on the surface of amino-functional Fe_3O_4 nanoparticles. The surface amino group of Fe_3O_4 particles could connect with rare-earth ions by N—Y(Eu)$^{3+}$coordination bond. The synthetic strategy as schematically illustrated in Scheme 1. With the excellent magnetic properties and surface amino functional groups of Fe_3O_4 cores, YVO_4:Eu^{3+} can be successfully deposited on their surface, so Fe_3O_4@YVO_4:Eu^{3+} bifunctional magnetic–luminescent nanocomposites with core–shell structure are synthesized. Compared with the synthesis of $Fe_3O_4/SiO_2/YVO_4$:$Eu^{3+}$and Fe3O4@nSiO2@mSiO2@YVO4:Eu3+ bifunctional nanocomposites reported by reference [49], our method is simple and the cost is low. In addition, without the coated SiO_2 layer, the prepared product has a good red emission and strong magnetic property.

2. Experimental

2.1. Reagents and characterization

Yttrium oxide (Y_2O_3, purity: 99.99%), europium oxide (Eu_2O_3, purity: 99.99%) were purchased from Shanghai Yuelong Non-Ferrous Metal Limited China, ammonium metavanadate (purity: 96.0%, NH_4VO_3), Ferric chloride hexahydrate (purity ≥99.0%, $FeCl_3·6H_2O$), ethylenediamine (purity ≥98.0%, $C_2H_8N_2$), sodium acetate (purity ≥99.0%, CH_3COONa), Ethylene glycol (purity 96.0%, EG), poly(ethylene glycol) (PEG *Mw* = 20,000) were purchased from Beijing Chemical Reagent Limited China. All chemicals are used without any further purification. Deionized water was used throughout experiment process.

Powder XRD patterns were obtained on a Bruker D&FOCUS X-ray powder diffraction (XRD) using Cu-Kα radiation (λ = 0.154056 nm). The morphologies and structures of the as-prepared samples were inspected on a JEM-2010-type transmission electron microscope (TEM). Fourier Transform IR spectra were recorded on a BRUKER Vertex 70 IR spectrophotometer using KBr pellet technique. The photoluminescence (PL) excitation and emission spectra were performed on a Hitachi F-4500 spectrofluorimeter equipped with a 150 W xenon lamp as the excitation source. Magnetization measurements were performed on an MPMS SQUID XL superconducting quantum interference device (SQUID) magnetometer at 300 K. All the measurements were performed at room temperature.

2.2. Synthesis of amino-functional magnetic Fe_3O_4 nanoparticles

Amino-functional magnetic Fe_3O_4 nanoparticles were prepared by the Solvent-thermal method [17]. Briefly, $FeCl_3·6H_2O$ (1.0 g) was dissolved in ethylene glycol (30 mL) to form a clear solution, followed by the addition of NaAc (2.0 g) and ethylenediamine (6.5 g). The mixture was stirred vigorously for 30 min and then sealed in a teflon-lined stainless-steel autoclave (50 mL capacity). The autoclave was heated to and maintained at 200 °C for 6 h, and then cooled to room temperature naturally. The black products were washed several times with ethanol and finally dried at 60 °C for 6 h. Then, the amino-functional Fe_3O_4 nanoparticles were obtained.

2.3. Synthesis of magnetic Fe_3O_4@YVO_4: Eu^{3+} nanocomposites

Eu^{3+}-doped yttrium vanadate (YVO_4:Eu^{3+}) luminescent shell was coated on the magnetic Fe_3O_4 nanoparticles by a direct precipitation method. In a typical procedure, 0.175 g of as-prepared Fe_3O_4 nanoparticles were dispersed in 38 mL of $Y(NO_3)_3$ and 2 mL of $Eu(NO_3)_3$ solutions. The mixture was sonicated for 20 min followed by the addition of 40 mL of 0.2 mol/L NH_4VO_3 solution, and then heated to 75 °C under vigorous mechanical stirring. After 2 h, the resultant products were separated with a magnet, thoroughly washed with ethanol and deionized water several times, and further dried at 60 °C overnight. The resulting magnetic Fe_3O_4@YVO_4:Eu^{3+} nanocomposites were obtained.

3. Results and discussion

3.1. Morphology and structure of the product

Pure Fe_3O_4 particles are prepared by a solvothermal process, consisting of monodisperse spherical nanoparticles with an average diameter of about 60 nm, a smooth surface and an apparent aggregation (Fig. 1a and b). The Fe_3O_4@YVO_4:Eu^{3+} particles are the spherical morphology, with non-aggregation, rough surface, and narrow size distribution. In addition, the core–shell structure can be clearly distinguished because of the different color contrast between the cores and shells. Fe_3O_4@YVO_4:Eu^{3+} are spheres with an average size of about 150 nm, and the shell shows a gray color

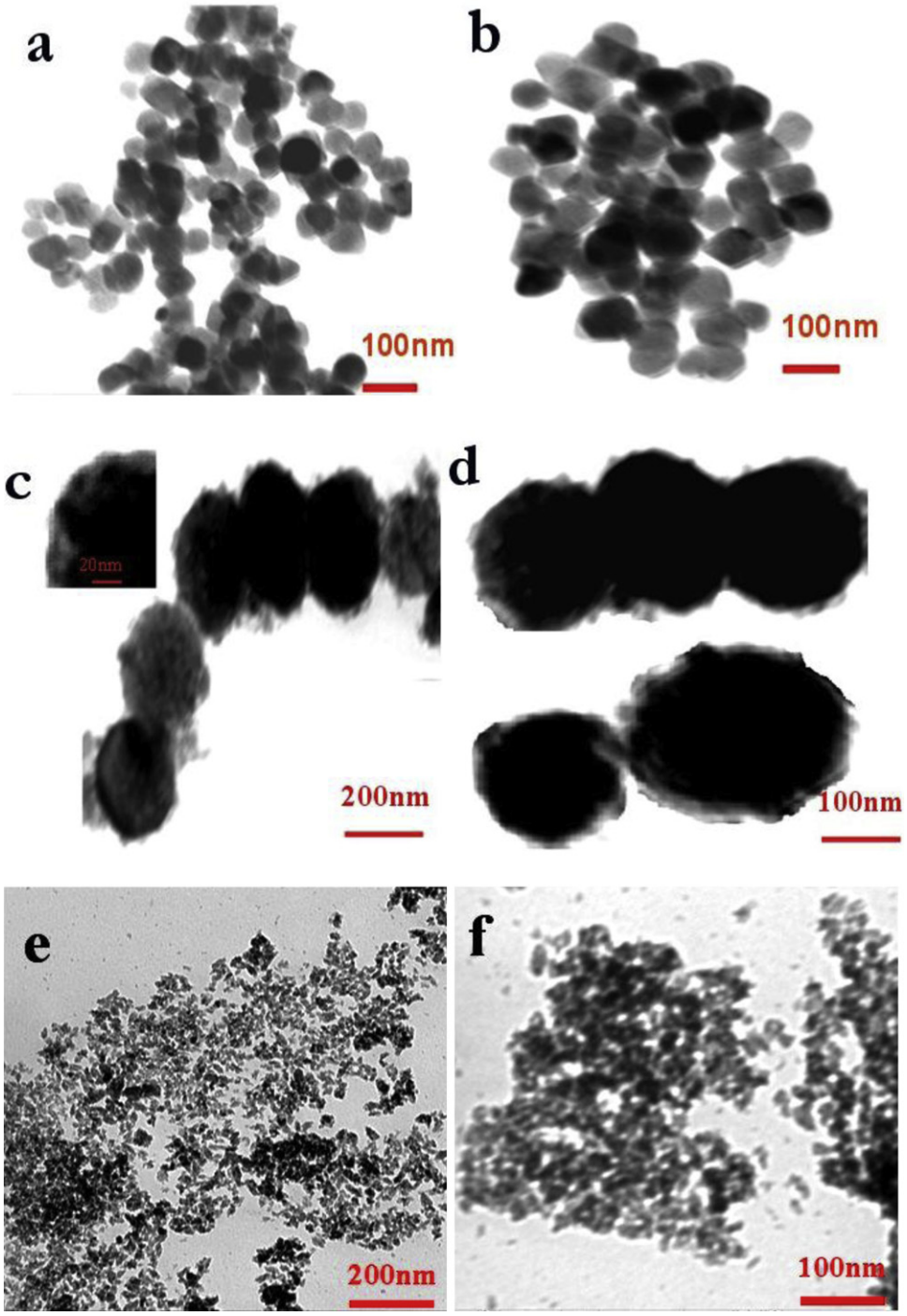

Fig. 1. TEM images of the Fe_3O_4 (a and b), Fe_3O_4@YVO_4:Eu^{3+} nanocomposites (c and d) and pure YVO_4:Eu^{3+} (e and f).

with an average thickness of about 15 nm (Fig. 1c and d). In most cases, each YVO_4:Eu^{3+} shell encapsulated more Fe_3O_4 nanoparticles. The change in diameter in Fig. 1a and c suggests that the YVO_4 nanocrystals deposited on the surface of Fe_3O_4 nanoparticles. Pure YVO_4:Eu^{3+} nanocrystals were prepared by a direct precipitation method, the obtained YVO_4:Eu^{3+} nanoparticles are spherical shape with an average diameter of about 20 nm (Fig. 1e and f).

In order to investigate the structure and composition of the nanocomposites, XRD was employed to analyze the samples. Fig. 2 shows the XRD patterns of pure Fe_3O_4 and Fe_3O_4@YVO_4:Eu^{3+} particles. From Fig. 2b, the magnetite core is easily indexed to cubic spinel structure of Fe_3O_4 (PDF 75-1610) with good crystallinity. In the case of Fe_3O_4@YVO_4:Eu^{3+} (Fig. 2d), besides the characteristic diffractions of cubic spinel Fe_3O_4 (marked with *), the obvious diffraction peaks at $2\theta = 25.0^\circ$, 34.0° and 49.5° can be indexed to the tetragonal phase of YVO_4 (PDF 17-0341, marked with°), which suggested the successful crystallization of YVO_4:Eu^{3+} on the surface of Fe_3O_4. Additionally, no additional peaks for other phases can be detected, which indicated that no reaction occurred between core and shell during the synthesis process.

The FT-IR spectra of Fe_3O_4, Fe_3O_4@YVO_4:Eu^{3+} and YVO_4:Eu^{3+} are given in Fig. 3. In the FT-IR spectrum of Fe_3O_4 (Fig. 3a), the absorption at 1644 cm^{-1} is attributed to the scissoring vibration absorption of N—H in the —NH_2, the band at 1392, 2926 cm^{-1} can

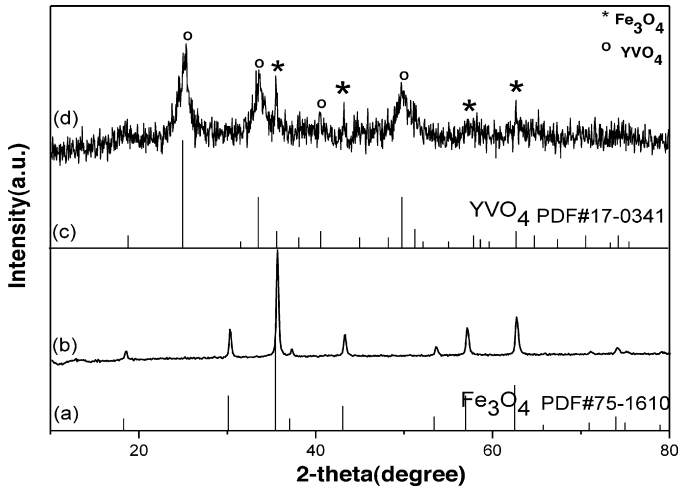

Fig. 2. XRD patterns of pure Fe_3O_4 (b), Fe_3O_4@YVO_4:Eu^{3+}(d), the standard date for magnetite Fe_3O_4 (a) and the standard date for YVO_4 (c).

be assigned to the asymmetric vibration absorption of C—H in the —CH_2, and the Fe—O vibration located at around 575 cm^{-1}[55]. Which confirmed that the ethylenediamine is successfully coated on the surface of Fe_3O_4 nanoparticles. At the same time, in the pattern of YVO_4 (Fig. 3c), the absorption around 807 cm^{-1} is assigned to VO_4^{3-} vibration [56]. Meanwhile, the absorption peaks around 1376, 1630 cm^{-1} are attributed to the residual NO_3^- absorption. The absorption peak around 3441 cm^{-1} is ascribed to —OH vibration. In the pattern of nanocomposites (Fig. 3b), besides the Fe—O vibration located at around 575 cm^{-1}, we can see obviously VO_4^{3-} vibration peak located at around 807 cm^{-1}. The FT-IR characterization results indicate that the YVO_4 has been successfully deposited onto the Fe_3O_4 nanoparticle surface.

3.2. Photoluminescence properties of the bifunctional nanocomposites

The PL properties of the pure YVO_4: Eu^{3+} and Fe_3O_4@YVO_4:Eu^{3+} samples were further characterized by excitation and emission spectra, as shown in Fig. 4. In the excitation spectra (Fig. 4A), the strong excitation band at 278 nm monitored with 617 nm emission of Eu^{3+} ($^5D_0$–$^7F_2$) can be assigned to the absorption of VO_4^{3-} group. No obvious f–f transition lines of Eu^{3+} can be found because of their

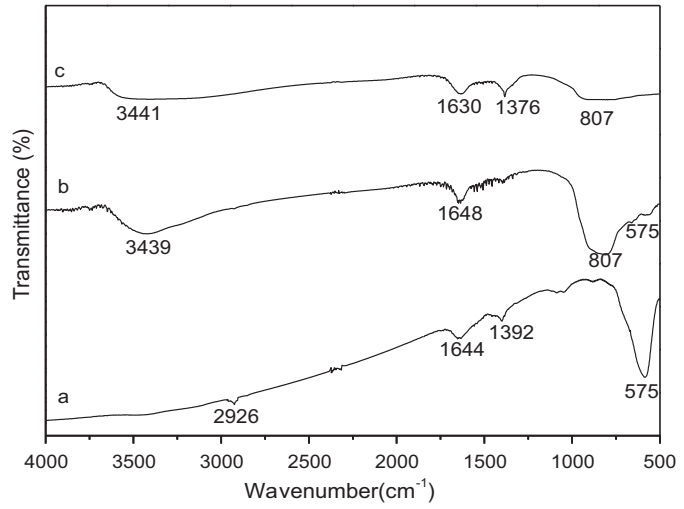

Fig. 3. FT-IR spectra of (a) Fe_3O_4, (b) Fe_3O_4@YVO_4:Eu^{3+} and (c) YVO_4:Eu^{3+}.

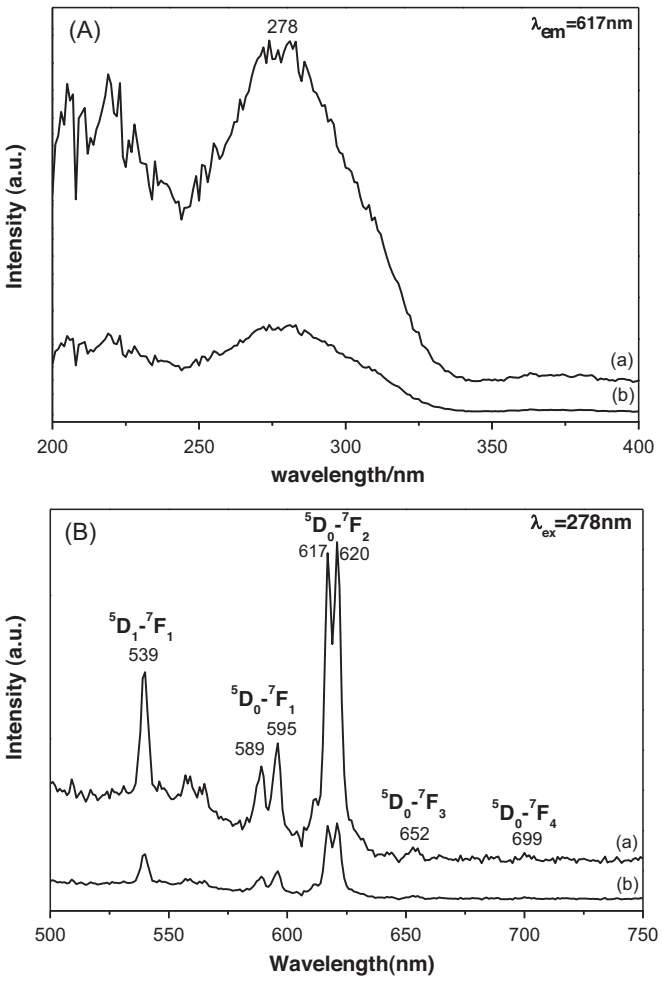

Fig. 4. Excitation (A) and emission (B) spectra of YVO_4:Eu^{3+} (a) and Fe_3O_4@YVO_4:Eu^{3+}(b).

low intensity with respect to that of VO_4^{3-}group, which indicated that the excitation of Eu^{3+} mainly results from the energy transform from VO_4^{3-} to Eu^{3+}. In the emission spectra (Fig. 4B) obtained by the excitation at 278 nm, the characteristic transition lines of Eu^{3+} ($^5D_{0,1}$–^7F_J, J = 1–4) can be observed. No emission lines from VO_4^{3-} groups are detected, which indicated an efficient energy transfer from VO_4^{3-} to Eu^{3+}. The characteristic peak in the red region originating from $^5D_0$–$^7F_2$ (617, 620 nm) transition is clearly dominant, which may be due to the low local symmetry (D_{2d}) for the sites of Eu^{3+} in the YVO_4 host lattices. Particularly, the characteristic emission and excitation peaks are still obvious except for the decreasing of intensity for Fe_3O_4@YVO_4:Eu^{3+} (curves b), which may be the reason of the direct contact between the luminescence YVO_4:Eu^{3+} and the black magnetite core. The results indicate that the as-prepared nanocomposites still possess good fluorescence in spite of the partial quenching by the black magnetite core [57].

3.3. Magnetic properties of the bifunctional nanocomposites

To investigate the magnetic properties of the Fe_3O_4 core and the Fe_3O_4@YVO_4:Eu^{3+} nanocomposites, the magnetization curves are shown in Fig. 5. Both samples exhibit a superparamagnetic behavior with a negligible coercivity or remanence, which indicated that the as-prepared sample is suitable for applications in drug delivery or separation. The saturation magnetization of Fe_3O_4@YVO_4:Eu^{3+} nanocomposites reaches a saturation moment of 34.8 emu/g, which is smaller than that of the Fe_3O_4 nanoparticles due to the decreased

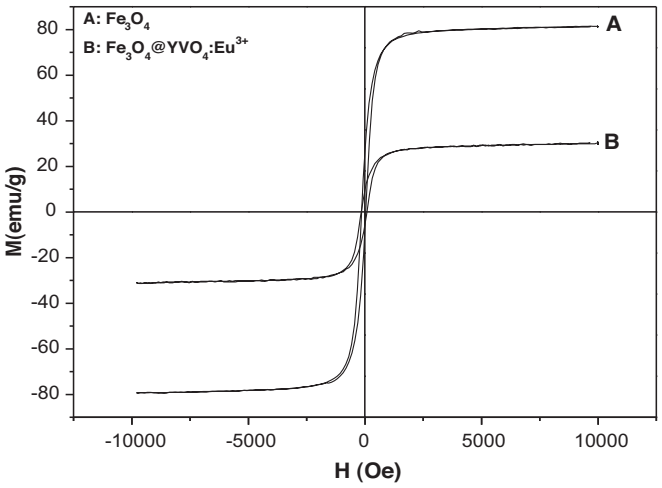

Fig. 5. Magnetization curves of Fe_3O_4 core (A) and Fe_3O_4@YVO_4:Eu^{3+} nanocomposites (B) at room temperature.

proportion of Fe_3O_4 in the nanocomposites. Although the saturation magnetization value of Fe_3O_4@YVO_4:Eu^{3+} nanocomposites decreased, the magnetization is still strong enough for the bioseparation and magnetic resonance imaging test.

4. Conclusions

In summary, we fabricated the Fe_3O_4@YVO_4:Eu^{3+} magnetic–luminescent nanocomposites by a facile direct precipitation process. The nanocomposites simultaneously exhibit excellent magnetic and luminescent properties and can be easily separated from solution using an external magnet. In a word, the magnetic and luminescent properties of the nanocomposites would allow them to find great potential applications in biomedical fields. Moreover, this simple method can extend to the fabrication of different types of bifunctional composites that can be used for a variety of bio-analytical assays.

Acknowledgment

This work was supported by the National Natural Science Foundation of P.R. China (NSFC) (grant no. 51072026) and the Development of science and technology plan projects of Jilin province (grant no. 20090528).

References

[1] S. Handa, V. Gnanadesikan, S. Matsunaga, J. Am. Chem. Soc. 132 (2010) 4925–4934.
[2] L.Y. Chen, C.L. Zhao, Y. Zhou, H. Peng, Y.Y. Zheng, J. Alloys Compd. 504 (2010) L46–L50.
[3] L.Y. Chen, Z. Lin, C.L. Zhao, Y.Y. Zheng, Y. Zhou, H. Peng, J. Alloys Compd. 509 (2011) L1–L5.
[4] C.L. Zhu, M.L. Zhang, Y.J. Qiao, J. Phys. Chem. C 114 (2010) 16229–16235.
[5] P. Guardia, A. Labarta, X. Batlle, J. Phys. Chem. C 115 (2011) 390–396.
[6] J. Ryu, H.Y. Park, K. Kim, J. Phys. Chem. C 114 (2010) 21077–21082.
[7] S.T. Selvan, T.T.Y. Tan, D.K. Yi, Langmuir 26 (2010) 11631–11641.
[8] G.X. Tong, W.H. Wu, J.G. Guan, H.S. Qian, J.H. Yuan, W. Li, J. Alloys Compd. 509 (2011) 4320–4326.
[9] H.M. Fan, M. Olivo, B. Shuter, J. Am. Chem. Soc. 132 (2010) 14803–14811.
[10] D.C. Niu, Z. Ma, Y.S. Li, J. Am. Chem. Soc. 132 (2010) 15144–15147.
[11] J. Chen, F.B. Wang, K.L. Huang, Y.N. Liu, S.Q. Liu, J. Alloys Compd. 475 (2009) 898–902.
[12] S.B. Ni, X.H. Wang, G. Zhou, F. Yang, J.M. Wang, Q. Wang, D.Y. He, J. Alloys Compd. 505 (2010) 727–732.
[13] L. Zhou, C. Gao, W.J. Xu, Langmuir 26 (2010) 11217–11225.
[14] K. Sobha, K. Surendranath, V. Meena, Biotechnol. Mol. Biol. Rev. 51 (2010) 1–10.
[15] Y. Chen, H.R. Chen, D.P. Zeng, ACS Nano 410 (2010) 6001–6013.
[16] M.A. Gonzalez-Fernandez, T.E. Torres, M. Andrés-Vergés, R. Costo, P. de la Presa, C.J. Serna, M.P. Morales, C. Marquina, M.R. Ibarra, G.F. Goya, J. Solid State Chem. 182 (2009) 2779–2784.
[17] H. Deng, X.L. Li, Q. Peng, Angew. Chem. Int. Ed. 44 (2005) 2782–2785.
[18] H. He, M.Y. Xie, Y. Ding, Appl. Surf. Sci. 255 (2009) 4623–4626.
[19] Q. Xiao, C. Xiao, Nanoscale. Res. Lett. 4 (2009) 1078–1084.
[20] J.S. Park, M.H. Yang, Y.H. Han, Mater. Chem. Phys. 104 (2007) 261–266.
[21] M.F. Zhang, S.J. Shi, J.X. Meng, J. Phys. Chem. C 112 (2008) 2825–2830.
[22] Z.H. Xu, C. Li, X.J. Kang, J. Phys. Chem. C 114 (2010) 16343–16350.
[23] R.D. Corato, N.C. Bigall, A. Ragusa, ACS Nano. Articles ASAP (As Soon As Publishable) doi:10.1021/nn102761t.
[24] J.W. Liu, Y. Zhang, C.Z. Yan, Langmuir 26 (2010) 19066–19072.
[25] R. Kas, E. Sevinc, U. Topal, J. Phys. Chem. C 114 (2010) 7758–7766.
[26] P. Sun, H.Y. Zhang, C. Liu, Langmuir 262 (2010) 1278–1284.
[27] X.L. Wang, L. Wei, G.H. Tao, Chin. Chem. Lett. 222 (2011) 233–236.
[28] L. Wang, K.G. Neoh, E.T. Kang, Biomaterials 31 (2010) 3502–3511.
[29] P. Lu, J.L. Zhang, Y.L. Liu, Talanta 822 (2010) 450–457.
[30] J. Fang, M. Saunders, Y.L. Guo, Chem. Commun. 46 (2010) 3074–3076.
[31] D.L. Zhao, X.X. Wang, X.W. Zeng, J. Alloys Compd. 477 (2009) 739–743.
[32] F. Erogbogbo, K.T. Yong, R. Hu, ACS Nano 49 (2010) 5131–5138.
[33] M.F. Wu, M.S. Wang, S.P. Guo, Cryst. Growth Des. 112 (2011) 372–381.
[34] Y. Wang, W.P. Qin, J.S. Zhang, J. Rare Earths 25 (2008) 605–608.
[35] S.L. Gai, P.P. Yang, C.X. Li, Adv. Funct. Mater. 20 (2010) 1166–1172.
[36] X.F. Zhang, L. Clime, H.Q. Ly, J. Phys. Chem. C 114 (2010) 18313–18317.
[37] H.C. Lu, G.S. Yi, S.Y. Zhao, J. Mater. Chem. 14 (2004) 1336–1341.
[38] Y.j. Jing, Y.H. Zhu, X.L. Yang, Langmuir 273 (2011) 1175–1180.
[39] Z.Y. Ma, D. Dosev, M. Nichkova, J. Mater. Chem. 19 (2009) 4695–4700.
[40] Y. Xu, A. Karmakar, D.Y. Wang, J. Phys. Chem. C. 114 (2010) 5020–5026.
[41] J.Q. Wan, H. Li, K.Z. Chen, Mater. Chem. Phys. 114 (2009) 30–32.
[42] B. Liu, W.X. Xie, D.P. Wang, Chem. Mater. Lett. 62 (2008) 3014–3017.
[43] Q. Zhang, J. Ding, Y.L. Shen, D.P. Chen, Q.L. Zhou, Q.X. Chen, Z.W. He, J.R. Qiu, J. Alloys Compd. 508 (2010) L13–L15.
[44] O. Veiseh, C. Sun, J. Gunn, Nano Lett. 5 (2005) 6–9.
[45] F. Grasset, F. Dorson, Y. Molard, Chem. Commun. 47 (2008) 29–31.
[46] Y.H. Deng, D.W. Qi, C.H. Deng, J. Am. Chem. Soc. 130 (2008) 28–31.
[47] Z.W. Sun, D. Liu, L.Z. Tong, Solid State Sci. 132 (2011) 361–365.
[48] L.Y. Wang, Z.H. Yang, Y. Zhang, J. Phys. Chem. C 113 (2009) 3955–3959.
[49] P.P. Yang, Z.W. Quan, Z.Y. Hou, Biomaterials 30 (2009) 4786–4795.
[50] Y.X. Zhang, S.S. Pan, X.M. Teng, J. Phys. Chem. C 112 (2008) 9623–9626.
[51] F. Vetrone, R. Naccache, V. Mahalingam, Adv. Funct. Mater. 19 (2008) 1–6.
[52] J. Wang, Y.H. Xu, M. Hojamberdiev, J. Alloys Compd. 481 (2009) 896–902.
[53] P. Huang, D.Q. Chen, Y.S. Wang, J. Alloys Compd. 509 (2011) 3375–3381.
[54] W. Chiu, P. Khiew, M. Cloke, J. Phys. Chem. C 114 (2010) 8212–8218.
[55] S.H. Huang, D.H. Chen, J. Hazard. Mater. 163 (2009) 174–179.
[56] J.B. Liu, H.M. Zhang, H. Wang, Chin. J. Inorg. Chem. 245 (2008) 777–780.
[57] Y.H. Li, Y.M. Zhang, P. Li, J. Func. Mater. Dev. 116 (2010) 74–76.